PERGAMON

Journal of Structural Geology 21 (1999) 437–448

JOURNAL OF STRUCTURAL GEOLOGY

A kinematic model for deformation within brittle shear zones

Trenton T. Cladouhos *

Department of Geological Sciences, Box 351310, University of Washington, Seattle, WA 98195, USA

Received 1 November 1996; accepted 11 December 1998

Abstract

Textural analysis of fault gouge indicates that displacement of particles within brittle shear zones occurs by three different modes: synthetic Riedel shears, antithetic Riedel shears, and shearing particulate flow. A kinematic model is developed which incorporates these three slip modes and constrains the combined deformation to be simple shear parallel to the shear zone boundaries. Penetrative fabric (P-foliation and shape preferred orientation of survivor grains) commonly observed in foliated fault gouge is assumed to be a result of the shearing particulate flow only. The model, which relates penetrative fabric orientation to the relative shear rates on Riedel shears and shearing particulate flow, reconciles inclined P-foliation and high ($\gamma > 10$) shear strain.

1. Introduction

Most upper crustal faults are filled with fault breccia and fault gouge formed by mechanical and chemical processes within the fault zone. Outcrop of gouge and breccia is notoriously poor as fault zones typically provide a weakness along which water seeps, streams flow, and vegetation grows. Consequently, structural descriptions of gouge and breccia are relatively rare. However, it is clear that the mechanics of fault zones and the seismic cycle are at least partially controlled by this material (Morrow and Byerlee, 1989; Marone et al., 1990, 1991). The turtleback faults on the east flank of southern Death Valley are superbly exposed, dry, and unvegetated, offering an ideal natural laboratory for studying the field geometry, kinematics, mechanics, and alteration within brittle shear zones (Fig. 1a).

Over 100 brittle fault rock samples have been collected from more than 30 locations along a detachment fault system at the eastern edge of southern Death Valley. Microstructural analysis of over 30 thin sections has led to a number of conclusions (Morgan and Cladouhos, 1995). Synthetic Riedel shears—marked by deflection of clay fabric, more intense comminution, and fractures—are present in a wide variety of fault rock types. Antithetic Riedel shears are notably rare. Clay-rich fault gouge commonly displays a P-foliation oriented ~165° from the shear plane. In fault gouge, the long axes of survivor grains—isolated, rounded clasts surrounded by finer grained matrix—define a profound shape preferred orientation (SPO) (Cladouhos, 1999). Some gouges and breccias contain a composite fabric defined by synthetic Riedel shears and a P-foliation (Fig. 1b and d), while other gouge types are characterized by a flow banding (Fig. 1c). These features are more thoroughly described elsewhere (Chester et al., 1985; Chester and Logan, 1986, 1987; Rutter et al., 1986; Moore et al., 1989) both in natural and experimentally deformed gouge and breccia. This paper develops a kinematic model of the deformation within brittle shear zones based on the microstructural features commonly observed in brittle fault rocks. This is done by writing tensor equations for three separate deformation modes—synthetic Riedel shears, antithetic Riedel shears, and shearing particulate flow—and then constraining the total deformation to be simple shear. I find a relationship between the steady-state orientation of P-foliation or

* Also at: Golder Associates Inc., 4104 148th Avenue NE, Redmond, WA 98052, USA.

E-mail address: tcladouhos@golder.com (T. Cladouhos)

0191-8141/99 $- see front matter
PII: S0191-8141(98)00124-2

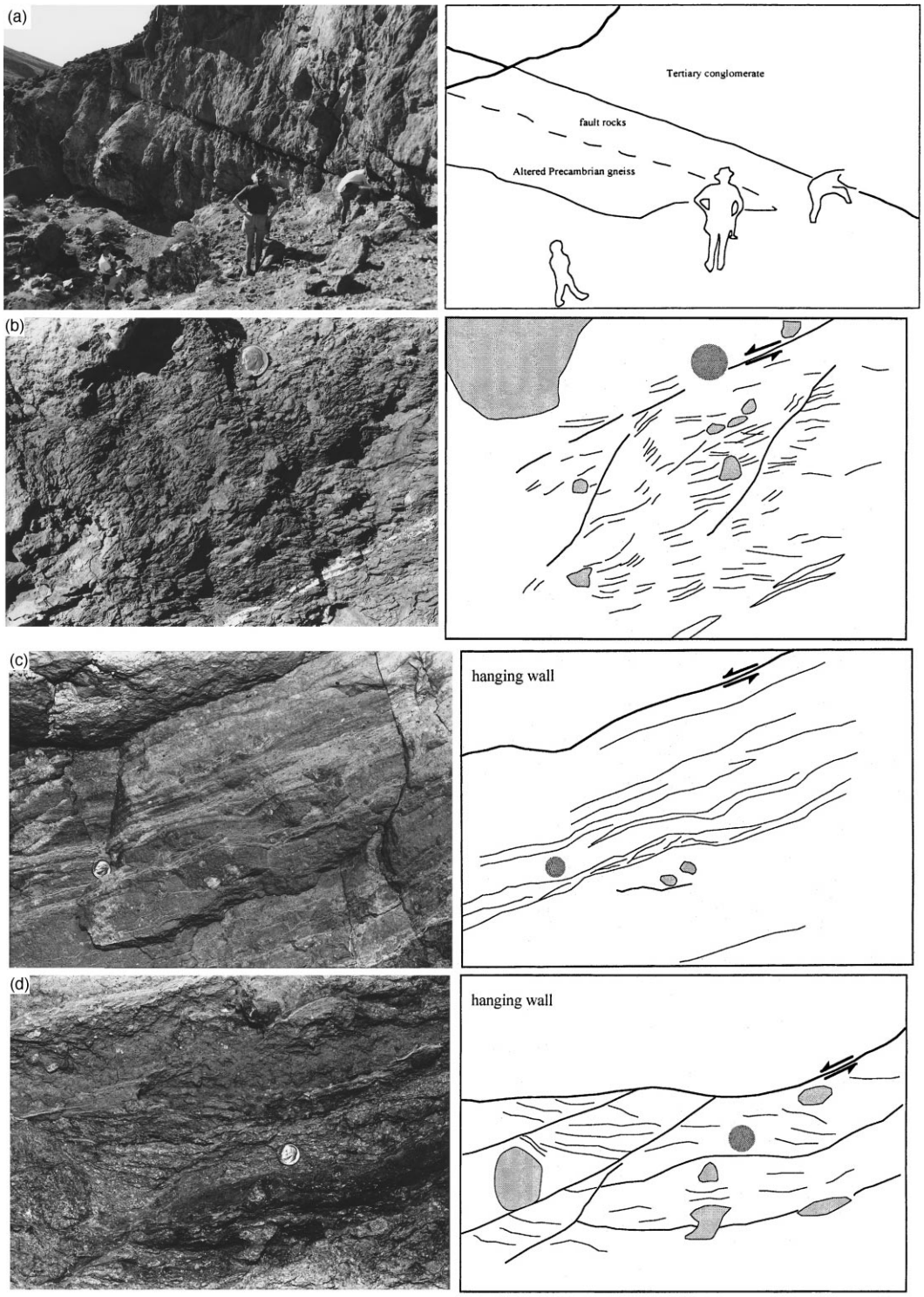

Fig. 1. (a) Outcrop photo of the Copper Canyon detachment fault. The distinct planar surface separates hanging wall conglomerate of the Miocene Copper Canyon formation from a zone of fault rocks. The lower boundary of the fault rock zone is more gradual. Below the fault rock zone (and on the horizon) are the Precambrian metamorphic rocks which give the range a smooth, gently curved form that resembles a turtle's back. (b) Outcrop photo of foliated clay gouge with P & R fabric. Riedel shears dip more steeply than the main fault plane (marked with sense of shear arrows). The dip of the P-foliation is variable in this photo; in some zones its dip is more shallow than the fault plane, and in other zones it is deflected toward localized slip surfaces. The bottom row of fig. 2 in Cladouhos (1999) shows microphotos of this type of rock. (c) Outcrop photo of flow-banded gouge. The banding is parallel to the main fault plane and is defined by boudinaged alternating green and tan layers. The middle row of fig. 2 in Cladouhos (1999) shows microphotos of the rock sampled from this location. (d) Outcrop photo of P & R fabric in fault breccia. Coarse foliation between Riedel shears is defined by crushed lenses of footwall rock. The top row of fig. 2 in Cladouhos (1999) shows microphotos of this type of rock.

SPO and the relative shear rates on the synthetic and antithetic Riedel shears and shearing particulate flow. This relation can be simply represented on a shear rate ternary diagram.

2. Background

Whether deformed at crystal–plastic or brittle conditions, rocks which have been deformed in shear zones commonly contain a composite planar fabric defined by localized slip surfaces (cisaillement or Riedel shears) and a continuous fabric (schistosity or P-foliation). Rocks deformed at high (>250°C) temperatures displaying this composite fabric are called *S–C* mylonites (Berthé et al., 1979; Lister and Snoke, 1984). Rocks deformed at lower temperature displaying the P & R composite fabric are called foliated cataclasites (Chester et al., 1985). Although many have suggested the use of composite planar fabrics as sense of shear indicators (i.e. Lister and Snoke, 1984; Rutter et al., 1986; Chester and Logan, 1987; Cowan and Brandon, 1994), the kinematic and mechanical significance of the feature is not understood.

It is intriguing that similar composite fabrics are observed in rocks deformed at a wide range of temperatures. In the last decade high temperature fault rocks (mylonites) have been well studied (e.g. Tullis et al., 1982; Hanmer and Passchier, 1991 and 213 references therein). In contrast, low temperature fault rocks (cataclasite, gouge, and breccia) have received relatively little attention (exceptions include Rutter et al., 1986; Chester and Logan, 1987; Petit, 1987). This paper will focus on fault rocks deformed at low temperatures although the ideas presented below are based upon kinematics and thus may be applicable regardless of deformation mechanism.

The first component of the composite planar fabric in foliated cataclasites is localized slip surfaces, defined by discontinuities, fractures, and shear bands oriented 10–20° to the primary shear plane (Fig. 2). These surfaces, called synthetic Riedel shears (Riedel, 1929; Skempton, 1966; Tchalenko, 1968), have been interpreted to be Coulomb slip surfaces (Mandl et al., 1977; Mandl, 1988, pp. 312–314). Their orientation ($\phi_i/2$) is related to the internal angle of friction ($\phi_i = 20$–$40°$) of the material. A second set of Coulomb slips (antithetic Riedel shears) can form oriented between 70 and 80° ($90° - \phi_i/2$) to the primary shear plane. Many rock experimentalists have adopted the model of Coulomb plasticity for deformation of gouge (Byerlee and Savage, 1992; Lockner and Byerlee, 1993; Beeler and Tullis, 1995). This means that the maximum principal stress and the infinitesimal strain directions are coaxial and oriented 45° to the shear zone boundaries. Slip occurs on sets of conjugate Coulomb shears which are symmetric about the principal strain directions and inclined to the main shear plane. If gouge volume is to be conserved and the shear zone walls are rigid, Coulomb plasticity requires equal total shear rates on both sets of synthetic and antithetic Riedel shears (Beeler and Tullis, 1995). The lack of observations of antithetic Riedel shears in natural gouges (e.g. Rutter et al., 1986; Chester and Logan, 1987) brings into question the validity of the Coulomb plasticity model. Indeed, the second component of the composite planar fabric is a foliation, not a set of antithetic Riedel shears.

In foliated cataclasites, the fabric is commonly defined by the preferred orientation of phyllosilicates and bands of mineral segregations (Rutter et al., 1986; Chester and Logan, 1987; Blanpied et al., 1995). The fabric can also be defined by shape preferred orientation (SPO) of survivor grains—large, rounded grains surrounded by a matrix of clay and other fine-grained material (Cladouhos, 1999). Although the orientations of these three independent elements (shape preferred orientations, phyllosilicate preferred orientations, and mineral segregations) may not be coincident, fabric elements inclined by 135–180° to the shear plane are collectively called P-foliation (Logan et al., 1979; Rutter et al., 1986). P-shears (Skempton, 1966; Logan

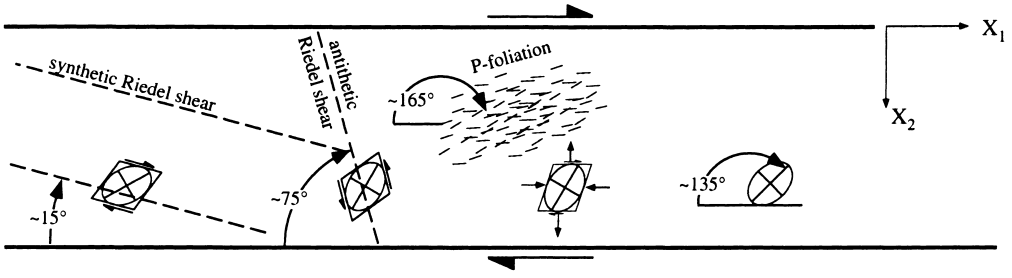

Fig. 2. Graphical representation of Eq. (6). The first and second ellipses from the left show the strain due to slip on synthetic and antithetic Riedel shears, respectively. The third ellipse shows strain accompanied by granular flow, which can include both pure shear and simple shear. The final ellipse shows the deformation required to maintain a constant shear zone thickness, which has principal axes oriented 45° to the shear zone boundary.

et al., 1979) have a similar orientation to the P-foliation and may be related, but they are distinct because the fabric records continuous deformation (granular or cataclastic flow) while the shears record discontinuous (localized) slip.

In contrast to Riedel shears, no model of development of the P-foliation has been proposed. Chester and Logan (1987) sampled foliated gouge from an exhumed spur of the San Andreas fault. They concluded that the March (1932) model for passive markers (Oertel, 1985) accurately explained two observations made at the microscopic scale: decrease in dispersion of clay mineral orientation and rotation of the mean orientation toward the shear plane with an increase in shear strain. In other words, Chester and Logan (1987) concluded that the fabric is strain-sensitive—it tracks the long axis of the finite strain ellipsoid—in foliated cataclasites (Means, 1981; Hanmer and Passchier, 1991). Using the March model, one can relate the finite shear strain across a shear zone to the orientation of the foliation (Fig. 3) (Ramsay and Huber, 1983). In field studies, foliations have been reported to be inclined by 135–180° (Rutter et al., 1986), and 142–19° (Chester and Logan, 1987). The shape preferred orientation of survivor grains reported in Cladouhos (1999) ranges from 160 to 10°. In laboratory studies, foliations have been reported to be inclined by 140–150° (Tchalenko, 1968), 140–180° (Chester et al., 1985), 150° (Rutter et al., 1986), and 150–160° (Moore et al., 1989). The shear strains experienced by the natural and simulated gouges in these studies are not well constrained; however, educated guesses of shear strain suggest that the March model does not properly explain the relation between foliation orientation and finite shear strain (Fig. 3). In particular, the inclination of the foliation in many natural rocks (Chester and Logan, 1987; Cladouhos, 1999) is too large given the high shear strains experienced by the fault gouges.

One explanation for the apparent departure from the March model is that strain is localized to very narrow zones within the fault gouge (Chester and Logan, 1987). If this is true, it is hypothesized that the inclined foliations formed when the entire gouge was deforming, and became fossilized as shear strain localized to very thin zones within the gouge. Another explanation, explored in this paper, is that the P-foliation is strain-insensitive (Means, 1981; Hanmer and Passchier, 1991); that is, it does not track the long axis of the finite strain ellipsoid. Cladouhos (1999) argues that the shape preferred orientation of survivor grains in fault gouge is strain insensitive, as rocks with apparently high shear strain have inclined SPO (Fig. 3).

3. The field study

Cladouhos (1999) describes the regional setting of the study area in Death Valley, California. I also provide details of how data on the preferred orientations of the survivor grains were collected using electron microprobe micrographs and an optical microscope. The primary conclusion of that paper is that survivor grains in fault gouge have a profound shape preferred orientation (SPO) that in some fault rock types is inclined to the shear plane. Cladouhos (1999) focuses on the penetrative deformation in fault gouge responsible for SPO and P-foliation. A more complete view of a brittle shear zone must also include the localized (non-penetrative) slip evidence in many thin sections and at the outcrop scale. In thin section localized slip surfaces are in orientations consistent with synthetic Riedel shears (Morgan and Cladouhos, 1995). In a granular material Riedel shears may not always leave a record, and their importance as a mode of deformation could easily be underestimated.

Cladouhos (1999) describes the three types of fault gouge identified in the field. A brief review of the distinguishing features of those types with special attention paid to their associated microstructures is necessary here as well. Fault breccia displays a coarse foliation defined by crushed lenses of footwall rock. Riedel shears are commonly visible in outcrop and thin section, giving fault breccia a composite P & R fabric (Lister and Snoke, 1984; Rutter et al., 1986; Chester and Logan, 1987; Cowan and Brandon, 1994) (Fig. 1d). Granular gouge is characterized by flow-banding defined by mineral segregations, foliation, or boudinaged clasts and layers (Fig. 1c). Significantly, Riedel shears have not been identified in granular gouge. The matrix is green–orange and composed of clay-sized grains, but not necessarily clay minerals. Clay gouge is clay-rich, brick-red–brown, foliated with dispersed millimeter sized clasts. Riedel shears are visible in thin sections in some clay gouge. Outcrop scale Riedel shears, along with the clay foliation, commonly give clay gouge a composite P & R fabric (Fig. 1b).

4. The model

4.1. Components of deformation

The following kinematic model of a shear zone includes the microstructural features observed within natural cataclasites; namely, P-foliation (including SPO), synthetic Riedel shears, and, for completeness, antithetic Riedel shears. I start by writing velocity gradients tensors (i.e. Bobyarchick, 1986) for each component. Plane strain (2D) and steady-state flow are assumed. Although the shear strain on localized slip

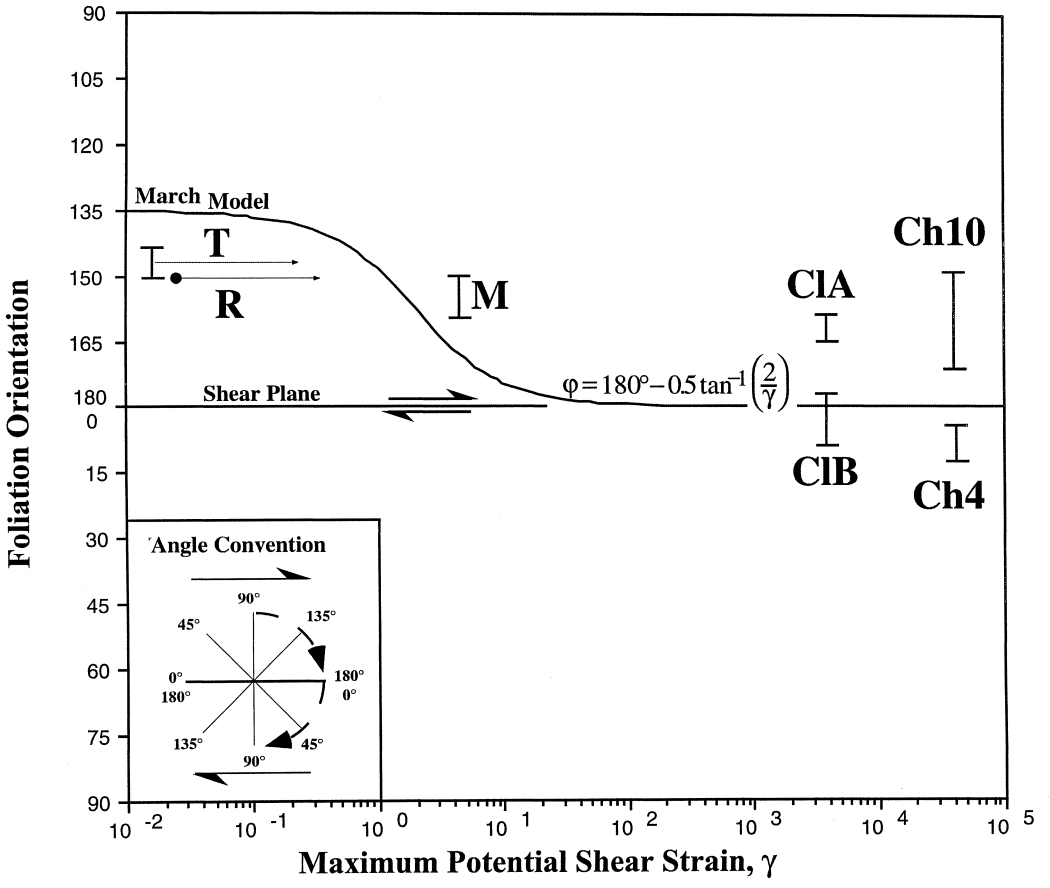

Lab Studies

R Rutter et al. (1986) "foliation formed at a few percent and remained stable at 30°"

M Moore et al. (1989) displ=2-3 mm, thickness=0.65 mm, γ≈4

T In the experiments of Tchalenko (1968) the fabric in sheared clays was considered to be a "compression texture" and hence the orientation thought to be unrelated to the finite strain.

Field Studies

Ch10 Chester & Logan (1987) sample DP10 displ=20 km, thickness=0.5 m, γ≈40000

Ch4 Chester & Logan (1987) sample DP4

ClB Cladouhos (1999): SPO range of flow-banded fault gouge, displ=2 km, thickness=0.5 m, γ≈4000

ClA Cladouhos (1999): SPO range of foliated clay gouge.

Fig. 3. March model annotated with field and laboratory data. Angle convention shown in inset. Shear strains for published data were calculated by dividing displacement by fault rock thickness.

surfaces (Riedel shears) is discontinuous and localized to narrow zones, concepts of fluid mechanics (i.e. the velocity gradients tensor) are applied; the shear displacement along a Riedel shear affects the flow path of the whole shear zone. The fluid mechanics assumption also implies that Riedel shears are ephemeral. As shear strain accumulates, both synthetic and antithetic Riedel shears will be rotated out of the ideal orientation, abandoned, and destroyed (Beeler and Tullis, 1995). New shears will reform at the angle specified by the internal angle of friction (ϕ_i). Preserved localized slip surfaces represent a snapshot of the total deformation and will not reflect the finite strain experienced by the gouge.

I choose a coordinate system with X_1 parallel to the fault zone boundary and X_2 perpendicular (Fig. 2). For the tensor components of strain, the convention that negative strains are contractional is used to be

consistent with Ghosh and Ramberg (1976). The instantaneous velocity field (Malvern, 1969, pp. 145–147) for a simple shear flow parallel to the X_1 axis is

$$\mathbf{L} = \dot{\gamma}\begin{bmatrix} 0 & 1 \\ 0 & 0 \end{bmatrix} \tag{1}$$

(Platt, 1984; Bobyarchick, 1986). This tensor represents a direct shear flow—flow parallel to the shear zone boundary—at a shear rate given by $\dot{\gamma}$. As discussed in the previous section, observations of the microstructures in natural fault rocks indicate that localized slip occurs on planes oblique to the shear zone boundary commonly called Riedel shears. The tensor equation that represents shear flow with rate $\dot{\gamma}_{R1}$ on planes inclined $\phi_i/2$ to the fault zone boundaries (synthetic Riedel shears, R1) is

$$\mathbf{L}_{R1} = \dot{\gamma}_{R1}\begin{bmatrix} \cos\frac{\phi_i}{2}\sin\frac{\phi_i}{2} & \cos^2\frac{\phi_i}{2} \\ -\sin^2\frac{\phi_i}{2} & -\sin\frac{\phi_i}{2}\cos\frac{\phi_i}{2} \end{bmatrix}. \tag{2}$$

Using the half angle formulas for sine and cosine and making a substitution for $\dot{\gamma}_{R1}$, Eq. (2) becomes

$$\mathbf{L}_{R1} = t\frac{\dot{\gamma}_{tot}}{2}\begin{bmatrix} \sin\phi_i & \cos\phi_i + 1 \\ \cos\phi_i - 1 & -\sin\phi_i \end{bmatrix} \tag{3}$$

where the scalar variable t is the ratio of the synthetic Riedel shear rate to the total shear rate ($\dot{\gamma}_{tot}$) across the fault zone.

Antithetic Riedel shears (R2) are Coulomb failure surfaces that make an angle of $90^\circ - \phi_i/2$ to the shear zone boundary and have a sense of shear opposite to the bulk shear on the zone. Substituting $90^\circ - \phi_i/2$ into Eq. (3) and reversing the sign of the shear gives the tensor components of the deformation occurring on antithetic Riedel shears:

$$\mathbf{L}_{R2} = v\frac{\dot{\gamma}_{tot}}{2}\begin{bmatrix} -\sin\phi_i & \cos\phi_i - 1 \\ \cos\phi_i + 1 & \sin\phi_i \end{bmatrix} \tag{4}$$

where the scalar variable v is the ratio of the shear rate on the antithetic Riedel to the total shear rate ($\dot{\gamma}_{tot}$) across the fault zone.

The final component of deformation within a fault zone is the distributed or granular flow which creates the features of mesoscopic ductility: oriented clasts, clay mineral foliation, and flow banding. In quantifying the deformation due to the Riedel shears, the flow was constrained to be simple shear. This constraint is not necessary for a continuous flow; therefore we allow for general shear deformation referenced to the shear zone boundary (Simpson and DePaor, 1993), the simultaneous combination of pure shear and simple shear. The strain rate ratio (s) is the ratio between pure shear and simple shear rates ($\dot{\varepsilon}/\dot{\gamma}$) (Ghosh and Ramberg, 1975). Then the tensor representation for the distributed flow becomes (Bobyarchick, 1986)

$$\mathbf{L}_P = u\frac{\dot{\gamma}_{tot}}{2}\begin{bmatrix} s & 2 \\ 0 & -s \end{bmatrix} = u\begin{bmatrix} \frac{\dot{\varepsilon}}{2} & \dot{\gamma}_{tot} \\ 0 & -\frac{\dot{\varepsilon}}{2} \end{bmatrix} \tag{5}$$

where again a scalar variable, u, is the ratio of this component to the total shear rate.

4.2. Solution

Because the tensors in Eqs. (3)–(5) represent the instantaneous velocity of particles, the components of each tensor can be summed to determine the total deformation within the fault

$$\mathbf{L}_{R1} + \mathbf{L}_{R2} + \mathbf{L}_P = \mathbf{D} + \mathbf{W}. \tag{6}$$

The right-hand side of Eq. (6) is shown decomposed into a symmetric stretching rate tensor (**D**) and an antisymmetric spin (or rotation rate) tensor (**W**) (Malvern, 1969; Bobyarchick, 1986). The components of the stretching rate tensor are specified if we assume that the fault zone thickness does not change over time:

$$\mathbf{D} = \frac{\dot{\gamma}_{tot}}{2}\begin{bmatrix} 0 & 1 \\ 1 & 0 \end{bmatrix}. \tag{7}$$

This tensor represents a strain rate in the fault gouge with principal axes oriented 45° to the shear zone boundary. The directions of no elongation are parallel and perpendicular to the shear zone boundary (zeros on the diagonals). The constraint of constant shear zone thickness is a reasonable first-order assumption; the significance of this assumption is further considered in the discussion section.

The tensor **W** describes a rigid body rotation of material lines with respect to the principal stretch axes. Unlike the stretching rate tensor, the components of the spin tensor are not uniquely specified. Instead the components of **W** can be arbitrarily scaled to the total shear rate by the variable, w:

$$\mathbf{W} = w\frac{\dot{\gamma}_{tot}}{2}\begin{bmatrix} 0 & 1 \\ -1 & 0 \end{bmatrix}. \tag{8}$$

To demonstrate that w is unconstrained, consider two end member solutions of Eq. (6). One solution is that of Coulomb plasticity: $\mathbf{L}_{R1} + \mathbf{L}_{R2} = \mathbf{D} + \mathbf{W}$. In this model, all deformation occurs on the Riedel shears which have equal shear rates (Beeler and Tullis, 1995). Setting $t = v$ and $u = 0$ (no distributed flow), and summing the components in Eqs. (3) and (4) we find

$$t\frac{\dot{\gamma}_{tot}}{2}\begin{bmatrix}0 & \cos\phi_i\\ \cos\phi_i & 0\end{bmatrix} = \frac{\dot{\gamma}_{tot}}{2}\begin{bmatrix}0 & 1\\ 1 & 0\end{bmatrix} + w\frac{\dot{\gamma}_{tot}}{2}\begin{bmatrix}0 & 1\\ -1 & 0\end{bmatrix} \quad (9a)$$

which is satisfied if

$$t = \frac{1}{\cos\phi_i} \text{ and } w = 0. \quad (9b)$$

In words, Coulomb plasticity achieves bulk pure shear of the gouge because the positive spin of the synthetic shears is canceled by the negative spin of the antithetic shears leaving a symmetric tensor.

Another solution to Eq. (6) is that of direct shear: $\mathbf{L_P} = \mathbf{D} + \mathbf{W}$. The components of this solution are found by setting the shear rates on the Riedels to zero ($t = v = 0$) and specifying the distributed flow to be simple shear ($s = 0$):

$$u\frac{\dot{\gamma}_{tot}}{2}\begin{bmatrix}0 & 2\\ 0 & 0\end{bmatrix} = \frac{\dot{\gamma}_{tot}}{2}\begin{bmatrix}0 & 1\\ 1 & 0\end{bmatrix} + w\frac{\dot{\gamma}_{tot}}{2}\begin{bmatrix}0 & 1\\ -1 & 0\end{bmatrix} \quad (10a)$$

which is satisfied if

$$u = 1 \text{ and } w = 1. \quad (10b)$$

In words, direct shear achieves the same stretching rate (**D**) as the Coulomb plasticity model; however, the spin component (**W**) is at a maximum.

Eqs. (9a)–(b) and (10a)–(b) represent just two end-member solutions to Eq. (6); w can take any value between 0 and 1. The family of possible combinations of the shear rate ratios can be found by solving for each component of strain. The elongation rate perpendicular to the shear zone (tensor indices of $i = 1, j = 1$) must be 0 to keep a constant shear zone width

$$t\sin\phi_i - v\sin\phi_i + us = 0. \quad (11a)$$

The shear strain rate parallel to the shear zone ($i = 1$, $j = 2$) is given by

$$t\cos\phi_i + t - v\cos\phi_i + v + 2u = 1 + w. \quad (11b)$$

And the shear strain rate perpendicular to the shear zone ($i = 2, j = 1$) is

$$-t\cos\phi_i + t + v\cos\phi_i + v = 1 - w. \quad (11c)$$

The result of Eq. (9b) suggests a change of variables to simplify Eqs. (11a)–(c)

$$T = t\cos\phi_i \quad (12a)$$

$$V = v\cos\phi_i \quad (12b)$$

and

$$U = u \quad (12c)$$

where $0 \le T \le 1$, $0 \le U \le 1$, and $0 \le V \le 1$ (instead of $0 \le t \le 1/\cos\phi_i$, $0 \le t \le 1/\cos\phi_i$). Substituting Eqs. (12a)–(c) into Eqs. (11a)–(c), and solving shows that the following three relations must be true:

$$s = \frac{V - T}{U}\tan\phi_i \quad (13a)$$

$$T + V + U = 1 \quad (13b)$$

and

$$w = \frac{T}{\cos\phi_i} - \frac{V}{\cos\phi_i} + U. \quad (13c)$$

4.3. The shear rate ternary, vorticity, and stable positions

Because the three deformation modes must add to unity [Eq. (13b)], a ternary diagram can be employed to graphically represent the rest of the solution. On the *shear rate ternary* (Fig. 4) each apex represents one of the three deformation modes, so that any point on the ternary represents a unique combination of the three components. On Fig. 4 the ratio between pure shear and simple shear rates (s), as given by Eq. (13a), is contoured. Strictly speaking the base of the ternary diagram cannot be occupied except at the center ($V = T$). Everywhere else along the base, $s \to \infty$ as $U \to 0$ [Eq. (13a)].

Eq. (13a) relates the ratio between pure shear and simple shear rates (s) within the distributed flow between Riedel shears to the relative shear rates of the

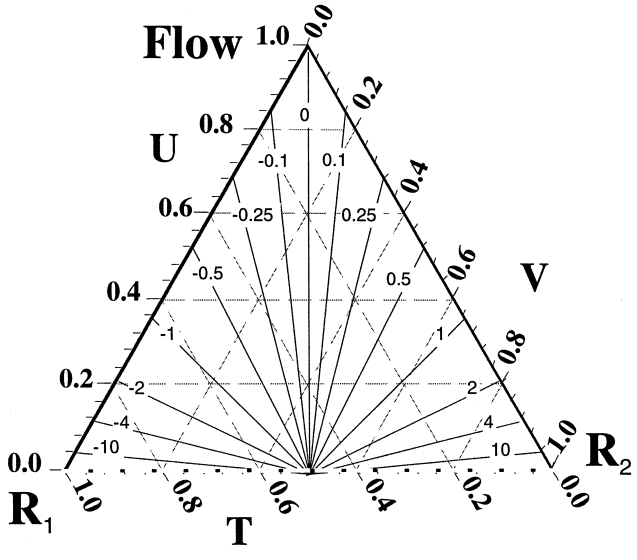

Fig. 4. Shear rate ternary with contours of the ratio of pure shear to simple shear rates (s). The relationship between the three apices and s is given by Eq. (13a). In this example, the internal angle of friction (ϕ_i) is 30°. The base of the ternary is dashed to indicate that $U = 0$ cannot be occupied (s is undefined) except at $V = T$.

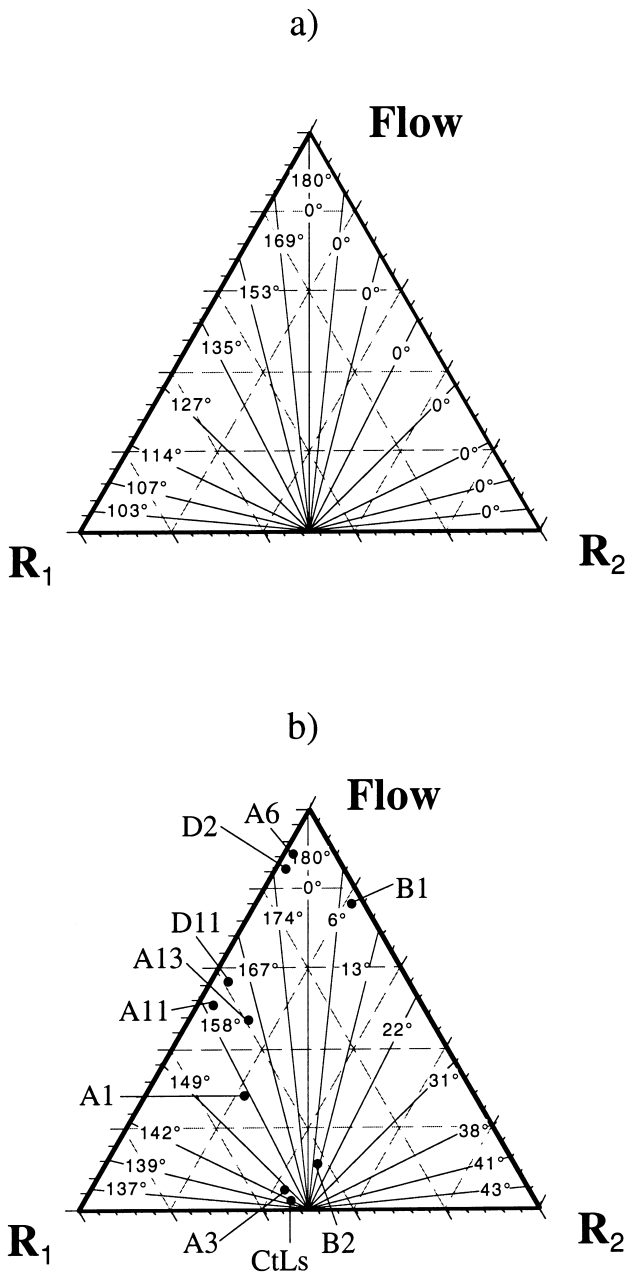

Fig. 5. (a) Shear rate ternary with contours for predicted elongate mineral foliation. On the left half of this ternary, the synthetic Riedel shears dominate ($T > V$), so the distributed flow between Riedel shears is thickening ($s<0$) and equation (4) from Cladouhos (1999) gives the stable eigenvector. On the right half of this ternary, the antithetic Riedel shears dominate ($V > T$), so the distributed flow between Riedel shears is thinning ($s > 0$) and equation (5) from Cladouhos (1999) gives the stable eigenvector. (b) Shear rate ternary with contours of predicted shape preferred orientation (SPO) of more equant clasts [see fig. 9 and equation (6) of Cladouhos, 1999]. Estimating the position of a fault rock on the shear rate ternary requires combining qualitative and quantitative data collected for each rock. The mean vector of the SPO data (i.e. fig. 7 and table 2 of Cladouhos, 1999) places a fault rock on a specific contour. To pin down the point along that contour, one must use a subjective assessment of the importance of antithetic Riedel shears compared to synthetic Riedel shears. For example, in samples A11 and D11 no R2 shears were observed; therefore, those samples plot near the R2 = 0 line.

shear components. This is an important connection because, as shown in Cladouhos (1999), this ratio will determine the preferred orientation of rigid bodies. Equations (4)–(6) of Cladouhos (1999) can be used to recast the contours of s shown in Fig. 4 to contours of stable positions of elongate clasts (Fig. 5a) and the mean vector of more equant clasts which continuously rotated (Fig. 5b). Then the mean vector of the SPO data presented in fig. 7 of Cladouhos (1999) can be plotted on the shear rate ternary (Fig. 5b) to give an estimate of the relative contributions of the three separate slip modes.

On the shear rate ternary the fault rocks analyzed fall into three groupings based upon a qualitative estimate of the importance of synthetic and antithetic Riedel shears and the orientation of the SPO mean vector (table 2 of Cladouhos, 1999). Flow-banded granular gouges plot near 100% particulate flow, consistent with SPOs that are roughly parallel to the shear plane and the absence of Riedel shears. The foliated clay gouges plot at 50–60% particulate flow and 40–50% synthetic Riedel shears, consistent with SPOs that are ~165° to the shear plane and the existence of some synthetic Riedel shears but lack of antithetic Riedel shears. Lastly, the breccias, plot near 50% synthetic and 50% antithetic Riedel shears, consistent with varied SPOs and deformation by Coulomb plastic cataclastic flow, not particulate flow.

4.4. Flow paths in general shear

The theoretical concept developed above can be further visualized by constructing models of particle paths for brittle shear zones. The constant shear zone thickness requirement [Eq. (7)] ensures that the *average* flow path for a particle must be parallel to the shear zone boundary regardless of the relative shear rates of the three slip modes. In detail, a particle's flow path will alternately be controlled by Riedel shears and granular flow. During offset on a Riedel shear, the particle path will have an orientation of $\varphi_i/2$, parallel to the secondary shear. During granular flow, the particle paths will depend upon the ratio of pure shear to simple shear rates in the general shear flow. Masuda et al. (1995) point out that the kinematical index angle

$$\Theta = \tan^{-1}(s) \tag{14}$$

gives the far-field matrix flow against the X_2 axis at ($X_2 = 0,\ X_1 = 1$). In this reference frame the velocity vector at every point will have an orientation of Θ. Thus it is straightforward to construct a flow-line model like those shown in Fig. 6 for any position on the shear rate ternary. The figure caption gives the details of the model's construction.

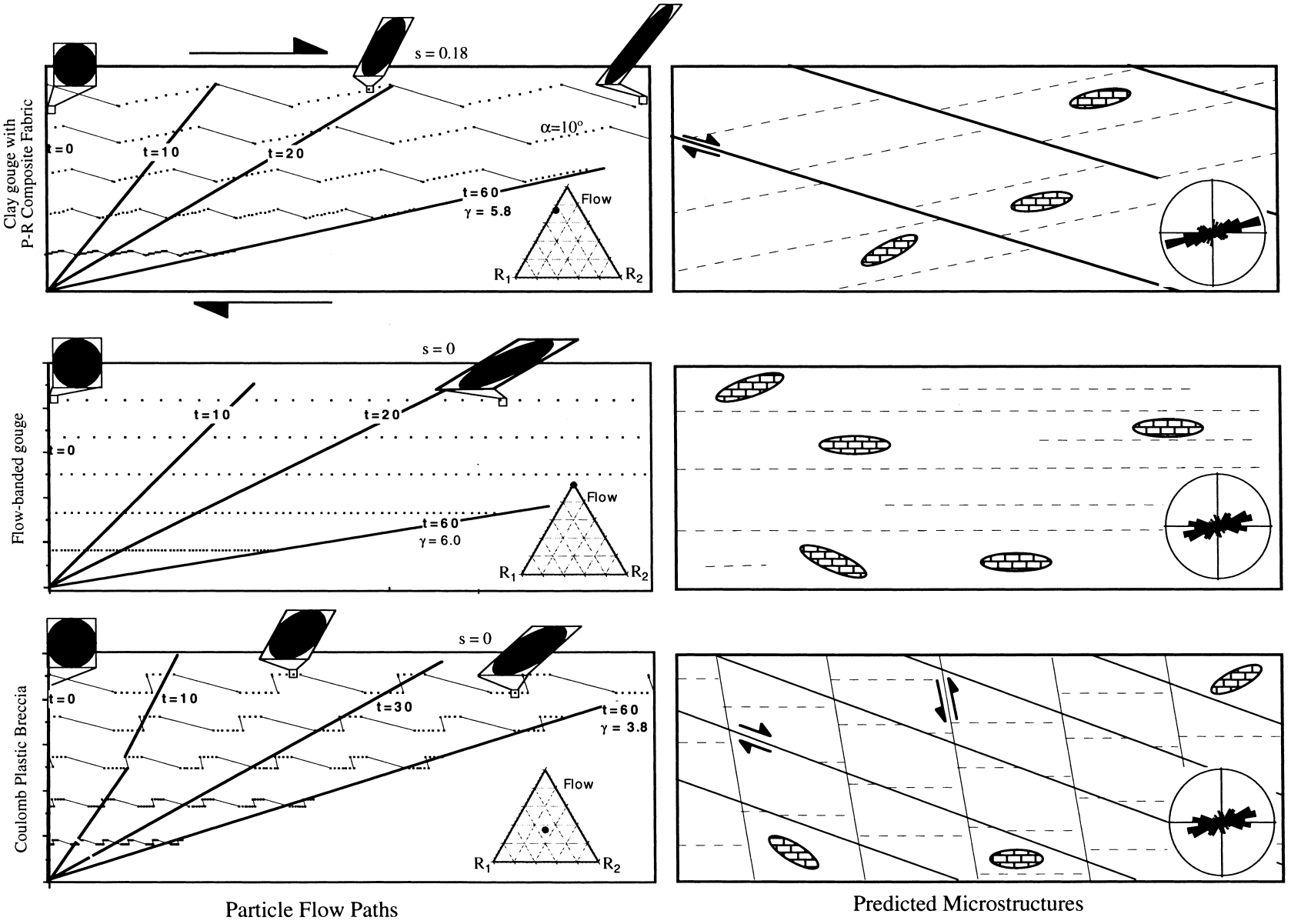

Fig. 6. Flow path models for three positions on the shear rate ternary. The left hand column shows the positions of five particles through time for three different positions on the shear rate ternary. Each sub-horizontal line represents the positions occupied by a particle that started at the left edge and traveled for 60 time steps. The bold lines labeled $t = 10$, $t = 20$, and $t = 60$ show the orientation of an originally vertical line after that many time steps. The sheared box and ellipse at the top of each model show the total penetrative strain partitioned to particulate flow. To construct the models with both Riedel shears and particulate flow it was assumed that every tenth time step a particle's path was controlled by a localized shear with a displacement of ten times the shear rate given by T or V. During the intervening nine time steps the particle path was controlled by the particulate flow in an orientation given by Eq. (14). The right hand column shows the microstructures predicted for the same combinations of T, U, and V. The rose diagrams showing the survivor grains SPOs were created by numerical modeling of the Ghosh and Ramberg (1976) model further described in Cladouhos (1999) (fig. 10). The flow paths with orientations Θ, shown as dashed lines, would be preserved as flow banding and striations on foliation surfaces. Note that the flow path orientations are not the same as the stable eigenvector orientations. The Riedel shears would be preserved as fractures, discontinuities, localized offsets of foliation, and deflection of clay fabric.

5. Uncertainties

Any model requires significant assumptions to be made in order to apply it to a natural situation. The kinematic model for brittle shear zones is no exception; therefore, a review of these assumptions and uncertainties is appropriate.

In applying Eq. (7), the shear zone thickness was explicitly assumed to be constant both in space and time. In my experience shear zone thickness *can* vary rapidly along dip and strike, in which case the assumption of Eq. (7) is invalid. Therefore, I must caution that the orientation of fabric and SPO in a fault rock sampled from a portion of a shear zone with local thickness changes would reflect the local shear zone geometry rather than the relative shear activities of the three components. This problem can be minimized by sampling for fabric and SPO analysis from regions with planar, parallel shear zone walls. To ensure a shear strain sufficient to develop or reset a fabric ($\gamma > 3$, i.e. fig. 9, Cladouhos, 1999), the region of constant thickness need only be about three times as long as the gouge is thick.

In addition to thickness changes, shear zones are heterogeneous with respect to several other physical parameters: for example, rock type, material properties, and fluid state. Therefore, it is worth asking whether a steady-state flow model is appropriate for a shear zone. While true steady-state is probably never achieved in a brittle shear zone, the relatively modest ($\gamma > 3$) shear strain necessary to reset a fabric means that only the last fraction of fault movement need be at steady conditions for the model to be appropriate.

Estimating the position of a fault rock on the shear rate ternary requires using the SPO orientation *and* a qualitative estimate of the relative shear activity of synthetic and antithetic Riedel shears (i.e. Fig. 5b). The shear activity estimate is complicated by the question of localized shear preservation. In a granular material, localized shear surfaces are marked by deflection of clay fabric, more intense comminution, and fractures. These features are ephemeral and would likely be erased by a small increment of shear. Furthermore, due to their high angle, the evidence for antithetic Riedel shears is likely to be erased faster than the evidence for synthetic Riedel shears. These considerations must be taken into account when estimating the relative importance of Riedel shears.

Figure 10 of Cladouhos (1999) shows that the mean vector of an SPO orbits about its average value by up to 15°. For example, in the case of simple shear (fig. 10b of Cladouhos, 1999) even after a shear strain of 10, the mean vector varies from 170 to 10°. The only solution to this problem is to collect multiple data sets from similar rocks. On average, the mean vector will correspond to the correct value of s.

6. Discussion and conclusion

The strengths of the model presented here are fourfold: (1) the model is kinematic, no fault rock rheology is assumed, (2) it is based upon observations of microstructures within fault gouge and breccia, (3) it explains inclined SPO and P-foliation in high strain gouge, and (4) it unites a bewildering variety of fabrics and textures into one model. Below I further elaborate on each of these strengths.

6.1. Kinematic model

The model employs instantaneous velocity gradient tensors [Eqs. (1)–(8)] to develop a kinematic description of particle movement in a brittle shear zone. The microstructures observed in fault gouge are given rheology-like attributes (Riedel shears are localized surfaces which do not contribute to the penetrative fabric, while the particulate flow leaves a record of clay foliation and shape preferred orientation); however, no attempt was made to relate axes and magnitudes of strain and stress. Instead, this approach links kinematic parameters [Eqs. (13a)–(b)] and flow paths (Fig. 6) to the observable microstructures. Eventually, it will be necessary to explore the mechanics implied by the kinematic model. Then perhaps the implications of mechanical and rheological models proposed by rock mechanists which predict the orientation of stress axes in laboratory-deformed gouge (i.e. Byerlee and Savage, 1992; Beeler and Tullis, 1995) can be better applied to understanding the kinematics and mechanics of natural fault zones.

6.2. Observational basis

Detailed observations of incohesive fault rocks found in upper crustal faults from Death Valley indicate that the breccia and gouge deformed by three different modes which, in combination, accomplished the simple shear necessary for fault movement. Recognition that these three deformation modes were roughly concurrent inspired the development of a kinematic model that includes synthetic Riedel shears, antithetic Riedel shears, and particulate flow. From the standpoint of explaining observational features of brittle shear zones, a three-mode kinematic model has two major advantages over the Coulomb plasticity model which only incorporates Riedel shears. First, the new model provides a mechanism, particulate flow, for developing clay mineral foliation, flow banding, and SPO of survivor grains. Second, in the Coulomb plasticity model, the total shear rates on synthetic and antithetic Riedel shears are required to remain equal in order to maintain constant shear zone thickness. In the new model, this requirement, which cannot be sup-

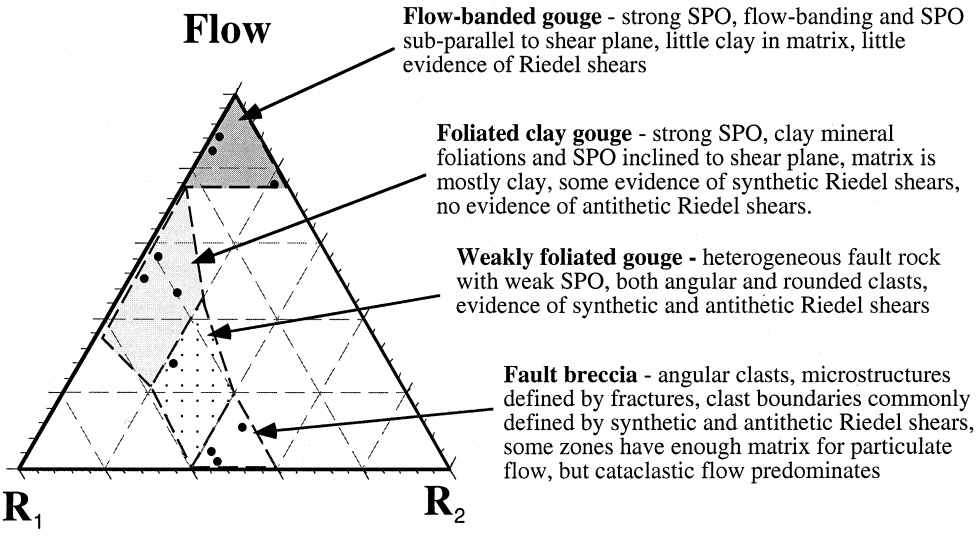

Fig. 7. Gouge textures and relative shear rates. This figure shows a proposed fault rock classification scheme based upon relative shear rates, gouge texture, and shape preferred orientation.

ported by observations of either natural or experimental gouges, is not necessary.

6.3. P-foliation paradox

Brittle fault rocks, especially clay gouge, commonly display a foliation defined by the preferred orientation of clay minerals, bands of mineral segregations, and the SPO of survivor grains. Traditionally the foliation orientation is assumed to be sensitive to the finite strain in cataclasites. This assumption raises a paradox. Based upon extreme comminution and roundness of survivor grains, many fault rock samples appear to have experienced high strains, but inclined foliations and SPO suggest low shear strains (Fig. 3 and Cladouhos, 1999). Another interpretation of the foliation orientation is that it is strain insensitive. The model developed in this paper provides the first quantitative model for a strain insensitive P-foliation. Further study of either natural or experimental gouge is necessary to determine conclusively which interpretation of P-foliation is correct.

6.4. Fault rock classification

Incohesive fault rocks and brittle shear zones defy simple classification. To the geologist unfamiliar with brittle deformation, each outcrop and hand sample appears to be unique. After making careful observations of the microstructures in outcrop and thin section, the shear rate ternary offers a scheme for classifying fault rock types (Fig. 7). The scheme links kinematics (the relative shear rates on Riedel shears and particulate flow) to textural and microstructural observations (foliation strength, flow banding, Riedel shear abundance, and shape preferred orientation and strength). As it is based upon microstructures and kinematics but leaves out fault rock source, alteration, and final composition, the shear rate ternary may not offer a complete classification scheme; however, it does indicate a kinematic distinction between clay gouge and granular gouge. Fine-grained granular gouge deforms without Riedel shears, and thus develops a shear-plane-parallel flow banding and SPO. Clay gouge does deform by displacement on synthetic Riedel shears and thus develops inclined foliation and SPO. The rheological or mechanical reason for this contrast in kinematic behavior is not currently known.

Acknowledgements

This work was performed under NSF grant #EAR-9417759 to Darrel S. Cowan. I thank D.S. Cowan and J.K. Morgan for their help throughout the project. Nick Beeler and Peter Hudleston provided valuable reviews of the manuscript.

References

Beeler, N.M., Tullis, T.E., 1995. Implications of Coulomb plasticity for the velocity dependence of experimental faults. Pure and Applied Geophysics 144, 251–276.

Berthé, D., Choukroune, P., Jegouzo, P., 1979. Orthogneiss, mylonite and non-coaxial deformation of granites: the example of the South Armorican Shear Zone. Journal of Structural Geology 1, 31–42.

Blanpied, M.L., Lockner, D.A., Byerlee, J.D., 1995. Frictional slip of granite at hydrothermal conditions. Journal of Geophysical Research 100, 13045–13064.

Bobyarchick, A.R., 1986. The eigenvalues of steady flow in Mohr space. Tectonophysics 122, 35–51.

Byerlee, J.D., Savage, J.C., 1992. Coulomb plasticity within the fault zone. Geophysical Research Letters 19, 2341–2344.

Chester, F.M., Logan, J.M., 1986. Implications for mechanical properties of brittle faults from observations of the Punchbowl Fault Zone, California. Pure and Applied Geophysics 124, 79–106.

Chester, F.M., Logan, J.M., 1987. Composite planar fabric of gouge from the Punchbowl Fault, California. Journal of Structural Geology 9, 621–634.

Chester, F.M., Friedman, M., Logan, J.M., 1985. Foliated cataclasites. Tectonophysics 111, 139–146.

Cladouhos, T.T., 1999. Shape preferred orientations of survivor grains in fault gouge. Journal of Structural Geology 21, 419–436.

Cowan, D.S., Brandon, M.T., 1994. A symmetry-based method for kinematic analysis of large-slip brittle fault zones. American Journal of Science 294, 257–306.

Ghosh, S.K., Ramberg, H., 1976. Reorientation of inclusions by combination of pure shear and simple shear. Tectonophysics 34, 1–70.

Hanmer, S., Passchier, C., 1991. Shear-sense indicators: a review. Geological Survey of Canada, Paper 90-17, 72 pp.

Lister, G.S., Snoke, A.W., 1984. *S–C* mylonites. Journal of Structural Geology 6, 617–638.

Lockner, D.A., Byerlee, J.D., 1993. How geometrical constraints contribute to the weakness of mature faults. Nature 363, 250–252.

Logan, J.M., Friedman, M., Higgs, N., Dengo, C., Shimamoto, T., 1979. Experimental studies of simulated gouge and their application to studies of natural fault zones. In: Proceedings of Conference VIII on Analysis of Actual Fault Zones in Bedrock: U.S. Geological Survey Open-File Report 79-1239.

Malvern, L.E., 1969. Introduction to the Mechanics of a Continuous Medium. Prentice-Hall, Englewood Cliffs, New Jersey.

Mandl, G., 1988. Mechanics of Tectonic Faulting. Elsevier, Amsterdam.

Mandl, G., de Jong, L.N.J., Maltha, A., 1977. Shear zones in granular materials—an experimental study of their structure and mechanical genesis. Rock Mechanics 9, 95–144.

March, A., 1932. Mathematische theorie der regelung nach der korngestalt bei affiner deformation. Zeitschrift für Kristallographie 81, 285–297.

Marone, C., Raleigh, C.B., Scholz, C.H., 1990. Frictional behavior and constitutive modeling of simulated fault gouge. Journal of Geophysical Research 95, 7007–7025.

Marone, C., Scholz, C.H., Bilham, R., 1991. On the mechanics of earthquake afterslip. Journal of Geophysical Research 96, 8441–8452.

Masuda, T., Michibayashi, K., Ohta, H., 1995. Shape preferred orientation of rigid particles in a viscous matrix: re-evaluation to determine kinematic parameters of ductile deformation. Journal of Structural Geology 17, 115–129.

Means, W.D., 1981. The concept of steady-state foliation. Tectonophysics 78, 179–199.

Moore, D.E., Summers, R., Byerlee, J.D., 1989. Sliding behavior and deformation textures of heated illite gouge. Journal of Structural Geology 11, 329–342.

Morgan, J.K., Cladouhos, T.T., 1995. Microstructures and fabrics of granular gouges from the Copper Canyon Detachment Fault, Death Valley. EOS 75 (46), F576.

Morrow, C.A., Byerlee, J.D., 1989. Experimental studies of compaction and dilatancy during frictional sliding on faults containing gouge. Journal of Structural Geology 11, 815–825.

Oertel, G., 1985. Reorientation due to grain shape. In: Wenk, H.-R. (Ed.), Preferred Orientation in Deformed Metals and Rocks: An Introduction to Texture Analysis. Academic Press, London, pp. 259–266.

Petit, J.P., 1987. Criteria for the sense of movement on fault surfaces in brittle rocks. Journal of Structural Geology 9, 597–608.

Platt, J.P., 1984. Secondary cleavages in ductile shear zones. Journal of Structural Geology 6, 439–442.

Ramsay, J.G., Huber, M.I., 1983. The techniques of modern structural geology. Academic Press, London.

Riedel, W., 1929. Zur Mechanik geologischer Brucherscheinungen. Centalblatt für Mineralogie, Geologie und Paläontologie 1929, 354–368.

Rutter, E.H., Maddock, R.H., Hall, S.H., White, S.H., 1986. Comparative microstructures of natural and experimentally produced clay-bearing fault gouges. Pure and Applied Geophysics 124, 3–30.

Simpson, C., DePaor, D.G., 1993. Strain and kinematic analysis in general shear zones. Journal of Structural Geology 15, 1–20.

Skempton, A.W., 1966. Some observations on tectonic shear zones. First Congress of the International Society of Rock Mechanics Proceedings, Lisbon, vol. 1, pp. 329–335.

Tchalenko, J.S., 1968. The evolution of kink-bands and the development of compression textures in sheared clays. Tectonophysics 6, 159–174.

Tullis, J., Snoke, A.W., Todd, V.R., 1982. Significance and petrogenesis of mylonitic rocks. Geology 10, 227–230.